Voltage-Controlled Spin-Wave Coupling in Adjacent Ferromagnetic-Ferroelectric Heterostructures

A. V. Sadovnikov,[1,2,*] A. A. Grachev,[1] E. N. Beginin,[1] S. E. Sheshukova,[1] Yu. P. Sharaevskii,[1] and S. A. Nikitov[1,2]

[1]*Laboratory "Metamaterials," Saratov State University, Saratov 410012, Russia*

[2]*Kotel'nikov Institute of Radioengineering and Electronics, Russian Academy of Sciences, Moscow 125009, Russia*

(Received 23 September 2016; revised manuscript received 7 December 2016; published 19 January 2017)

We experimentally study the spin-wave coupling in adjacent ferrimagnetic-ferroelectric heterostructures. By using the space-resolved Brillouin light-scattering spectroscopy, we perform a systematic study of the coupling of waves propagating in both a magnetic and a ferroelectric layer. We demonstrate the voltage-controlled transfer of the spin-wave energy between the adjacent bilayers. Our results show, that the coupling efficiency of the proposed laterally coupled multiferroics can be tuned by independent variation of the applied magnetic and electric field, which opens exciting prospects for an emerging field of magnonics.

DOI: 10.1103/PhysRevApplied.7.014013

I. INTRODUCTION

Recent progress in magnon-based electronics shows that a spin wave can be used as a signal carrier in the magnonic waveguide structures operating in the gigahertz and terahertz frequency range [1–5]. Composite structures consisting of ferrimagnetic and ferroelectric layers have aroused tremendous interest in the scientific community over the years due to their improved properties compared to those of the individual layers [6–13]. Such layered heterostructures provide us with unique opportunities for theoretical and experimental studies on magnetoelectric coupling. The latter leads to the possibility of tuning the magnetic properties with an electric field, and vice versa. Dual H-field and E-field tunability is the key advantage of ferromagnetic-ferroelectric heterostructures operating at room temperature. Magnetic tuning can be performed through the variation of a bias magnetic field, while electric tuning is possible due to control of the properties of ferroelectric layer through the variation of an applied electric field [14–16], which causes the change of dielectric permittivity of the ferroelectric layer.

The revival of interest in multiferroic heterostructures has been primarily driven by important potential applications in micro- and nanosized functional devices. The formation of the gradient of a magnetic and electric field [17,18] in multiferroic heterostructures allows one to be effectively used as a building block in the inherently scalable magnonic architecture [4]. Recently significant attention has focused on tunable magnonic couplers and beam splitters, which are the universal magnonic components suitable for versatile operations with data in magnonic networks [19–22]. The integration of magnonic structures with ferroelectric opens a promising alternative to signal processing by spin waves. However, the coupling mechanism in side-coupled multiferroic bilayers has been elusive. Our studies of the properties and wave dynamics in the coupled multiferroics were originally motivated by their promising features, which have the potential to provide beyond-CMOS computing technology [3,4,23,24] with decreased energy consumption.

Here, we report on an experimental investigation of spin-wave coupling in an adjacent ferromagnetic-ferroelectric heterostructure bilayer. The latter is composed of a barium strontium titanate slab and insulating thin-film ferrimagnet yttrium iron garnet film. We show the efficient voltage-controlled transfer of the spin-wave energy between the adjacent bilayers. We demonstrate by numerical simulation the hybridization of eigenmodes of adjacent magnetic stripes with transverse modes of a ferroelectric slab. We report on Brillouin light scattering and microwave measurements, displaying the effective tuning of coupling length via both the magnetic and the electric field. These results are important for the development of integrated magnetic devices with dual tunability in the framework of alternative wave-based magnonic computing concepts.

Our paper is organized as follows. In Sec. II, we present the experimental details of fabrication as well as microwave and Brillouin light-scattering characteristics of the coupled multiferroic structure. In Sec. III, we reveal the mechanism of the hybrid spin-electromagnetic wave coupling in the side-coupled bilayer stripes. We conclude with a discussion in Secs. IV and V.

II. SIDE-COUPLED MULTIFERROIC BILAYER

Figure 1(a) shows the schematic of laterally coupled bilayers. The magnetic layer is fabricated with the patterning [25] of the insulating thin-film ferrimagnet yttrium

*sadovnikovav@gmail.com

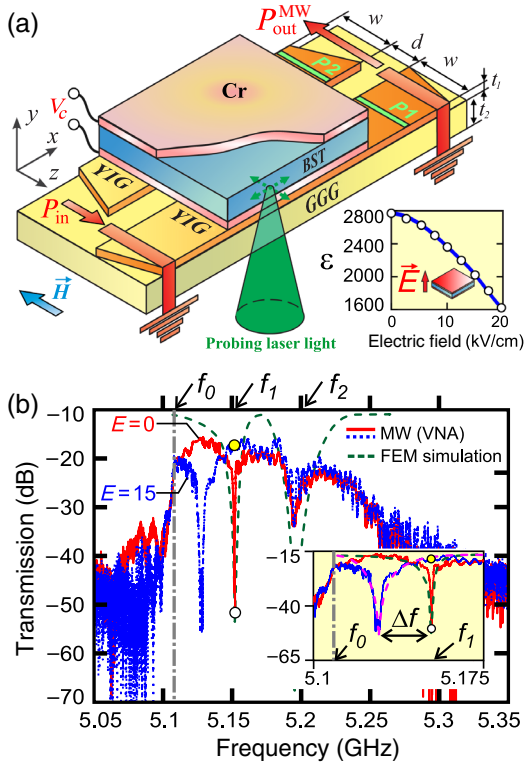

FIG. 1. (a) Schematic view of the bilayer heterostructure. A BLS measurement is performed in a backscattering configuration. A probing laser beam is focused from the polished GGG side. (Inset) Dielectric permittivity of BST, measured at different values of the electric field. (b) Transmission for port P_1 for different levels of a static electric field (red solid curve, 0 kV/cm; blue dashed curve, 15 kV/cm). The calculated transmission is shown as a dashed green curve. (Inset) Scaled region of a voltage-induced frequency shift of a transmission dip.

iron garnet [(YIG), $Y_3Fe_5O_{12}(111)$] into the form of side-coupled stripes with edge-to-edge spacing of $d = 40$ μm. YIG film with a thickness of $t_1 = 7.7$ μm and a saturation magnetization of $M_0 = 140$ G is epitaxially grown on a $t_2 = 500$ μm thick gadolinium gallium garnet [(GGG), $Gd_3Ga_5O_{12}(111)$] substrate. The reverse side of GGG is optically polished to provide the Brillouin light-scattering (BLS) measurement in the backscattering configuration [26]. It is convenient to denote the magnetic stripes by S_1 and S_2. The width of both stripes is $w = 210$ μm. We separate a 450-μm-thick ceramic barium strontium titanate [(BST), $Ba_{0.6}Sr_{0.4}TiO_3$] slab with the in-plane dimension of 5×0.46 mm from the YIG layer by a 30-nm-thick chromium (Cr) electrode, which is deposited on the surface of BST. The thickness of the Cr electrode is smaller than the skin depth for microwaves over the frequency range up to 10 GHz [27–31]. A 40-μm-thick Cr electrode is attached to the top of the BST. Owing to a sufficiently thick BST slab, the upper Cr electrode has no effect on spin-wave propagation in YIG. The electric voltage V_c in the range 0–900 V (an electric field) is applied to Cr electrodes in order to change the electric permittivity of the BST layer $\varepsilon(E)$. The electric field in BST varies within the range $E = 0$–20 kV/cm. This range leads to a variation of the permittivity [see the inset in Fig. 1(a)].

First, we analyze the transformation of transmission response of the test device when varying the applied electric field E from 0 to 15 kV/cm. The sample is placed into the uniform static magnetic field $H = 1200$ Oe oriented along the z axis for effective excitation in stripe S_1 of a guided magnetostatic surface wave (MSSW), also referred to as Damon-Eshbach (DE) spin waves [32–34]. The lateral confinement of both magnetic stripes leads to a reduction of the internal magnetic field in the DE configuration. Thus, the internal field at the center of the waveguide is $H_i = 1148$ Oe.

The principle of the tested structure operation is as follows. Excitation of a MSSW in the stripe S_1 is performed with the 50-Ω-matched microstrip transmission line with microwave transducers 30 μm wide and 1 mm long. As the spin wave propagates along the x direction, it is transformed to a hybrid spin-electromagnetic wave (HSEW) in the region where both YIG stripes are in contact with the BST slab. The HSEW propagates along the coupled stripes S_1 and S_2, loaded with BST as a superposition of symmetric and antisymmetric modes [19,21] of the adjacent magnetic stripes. The output transducer is also attached to S_1 at a distance of 6 mm from the input transducer [see Fig. 1(a)]. Thus, the HSEW reaches the area of YIG stripes without BST, where it is transformed back into a MSSW and is received by the output microstrip transducer [27,28,31].

The transmission response (the absolute value of S_{21} parameter) of the MSSW in the tested device is measured by a microwave (MW) technique using the E8362C PNA network analyzer. The experiments are performed at the relatively small input MW power $P_{in} = 0.1$ μW corresponding to the linear regime of the MSSW propagation in the YIG film [34]. The solid red line in Fig. 1(b) shows the measured absolute value of S_{21} when no electric field is applied ($E = 0$ kV/cm). Two well-pronounced stop-band dips, denoted by $f_1 = 5.15$ GHz (a 30-dB drop) and $f_2 = 5.19$ GHz (a 10-dB drop) in Fig. 1(b), correspond to the frequencies, at which the power of the HSEW does not effectively return to the stripe S_1 [21]. Thus, the side-coupled multiferroics can act as the frequency-filtering element, similar to that found in Ref. [35]. When the applied electric field is increased from 0 to 15 kV/cm, the central frequency of the first stop-band dip exhibits a redshift at $\Delta f = 25$ MHz [see the inset in Fig. 1(b)]. This result is demonstrated by the blue curve in Fig. 1(b). Here, the frequency of first dip is denoted by f_1. The gray vertical dashed-dotted line denotes the frequency of the ferromagnetic resonance [36] $f_0 = \gamma\sqrt{H_i(H_i + 4\pi M_0)}$, where $\gamma = 2.8$ MHz/Oe is the electronic gyromagnetic ratio for YIG.

Second, to demonstrate the efficient coupling between multiferroics and to prove the nature of the dip in

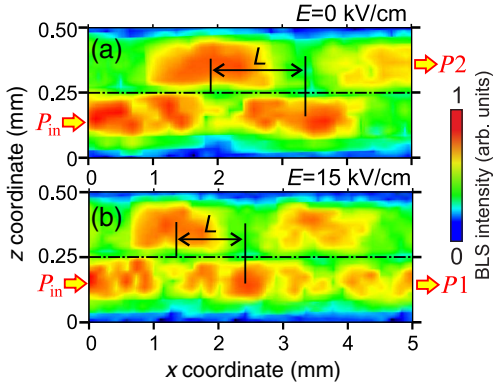

FIG. 2. Normalized color-coded BLS intensity map recorded at (a) $E = 0$ kV/cm and (b) $E = 15$ kV/cm at the excitation frequency of f_1. All of the shown data are obtained at $H = 1200$ Oe.

transmission response, the detection and spatial mapping of the HSEW intensity is performed by using the BLS technique [26,37,38] and by scanning the probing light spot along the x and z axes with a spatial resolution of 20 μm. Figure 2 shows the pseudo-color-coded two-dimensional 5×0.5 mm^2 spatial maps of the recorded BLS intensity $I(x, z)$ at the frequency f_1. When comparing the maps for $E = 0$ kV/cm [Fig. 2(a)] and $E = 15$ kV/cm [Fig. 2(b)], one should note that the power of the HSEW is transferred from S_1 to S_2 in a periodic manner with the spatial period $2L$, which is tuned by the value of the applied electric field. Here, L is the coupling length [21,39], i.e., the distance necessary to fully transfer the power from S_1 to S_2. Thus, owing to the signal switching from port P_1 at $E = 0$ kV/cm to port P_2 at $E = 15$ kV/cm, the coupled multiferroics demonstrate electric-field tunability.

III. MECHANISM OF HSEW COUPLING IN SIDE-COUPLED MULTIFERROIC STRIPES

Next, to elucidate the reason of the observed switching of HSEW power, we compare the dispersion of the wave propagated in the coupled multiferroics and the coupled magnetic stripes [21]. We demonstrate in Fig. 3(a) the dispersion of MSSW in the coupled stripes without a BST layer in order to obtain the reference characteristics (the open squares). With open triangles, we plot the dispersion of the HSEW in the tested coupled multiferroic structure. To analyze the shift of the dispersion curve (the differences between the coupled MSSW and the coupled HSEW), we use the finite-element method (FEM) [40,41], which provides the electrodynamic characteristics of both the MSSW and the HEMSW. The dotted curves in Fig. 3(a) show the calculated dispersion for symmetric (k_1^s) and antisymmetric (k_1^{as}) MSSW modes (in the coupled stripes without BST). The distribution of the E_z component for these modes is depicted in Figs. 3(f) and 3(e). In the

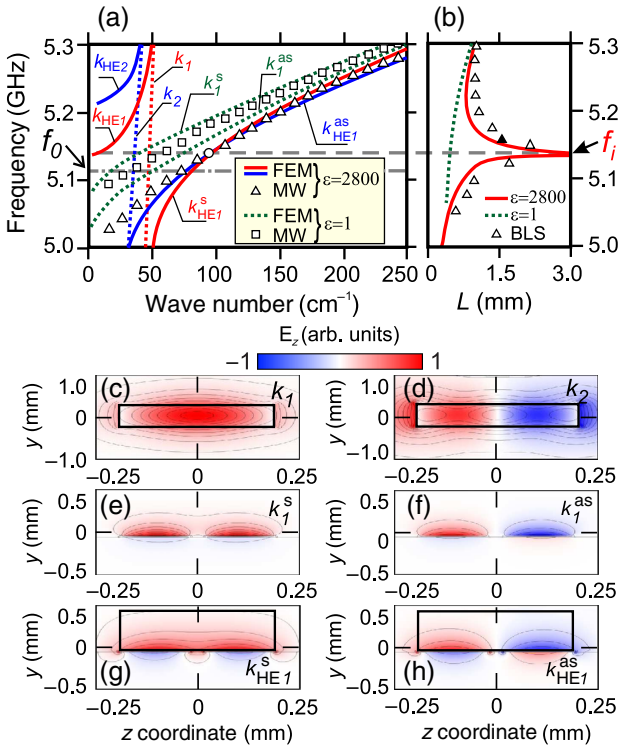

FIG. 3. FEM calculation results for (a) dispersion characteristics and (b) frequency dependence of the coupling length for symmetric and antisymmetric modes in coupled magnetic stripes (the dotted curves) and coupled multiferroics (the solid curves). Open squares and triangles denote the experimental data. The horizontal gray dashed-dotted line marks the frequency f_0, while the dashed line denotes the frequency f_i. Profiles of the (c) first and (d) second modes of the TE electromagnetic wave of the BST slab. Profiles of symmetric and antisymmetric modes in (e),(f) a coupled YIG film and (g),(h) a YIG/BST bilayer. Frames of the BST layer are outlined with a rectangle. Borders of the YIG film are not depicted due to the small thickness (in the current figure scale). The data are calculated for the frequency of f_1 and $H = 1200$ Oe.

coupled multiferroic structure, the symmetric mode k_1^s and the antisymmetric mode k_1^{as} are coupled to the first [k_1, Fig. 3(c)] and second [k_2, Fig. 3(d)] eigenmodes of the slow transverse-electric (TE) electromagnetic wave in the BST slab, respectively. We emphasize that we consider only the first width modes of each magnetic stripe [42,43] and two lower-order modes of the BST slab [39] to establish the theoretical models which can describe the behavior of the side-coupled multiferroics. The hybridization of the waves in the magnetic stripes and the BST slab leads to the splitting of the dispersion curves of both the symmetric and antisymmetric modes, which is demonstrated in Fig. 3(a) by the solid lines. Therefore, a coupled multiferroic structure can propagate both a slow wave with a transverse-electric polarization in a BST slab (k_{HE1}, k_{HE2}) and a symmetric [k_{HE1}^s, Fig. 3(g)] and an antisymmetric [k_{HE1}^{as}, Fig. 3(h)] HSEW.

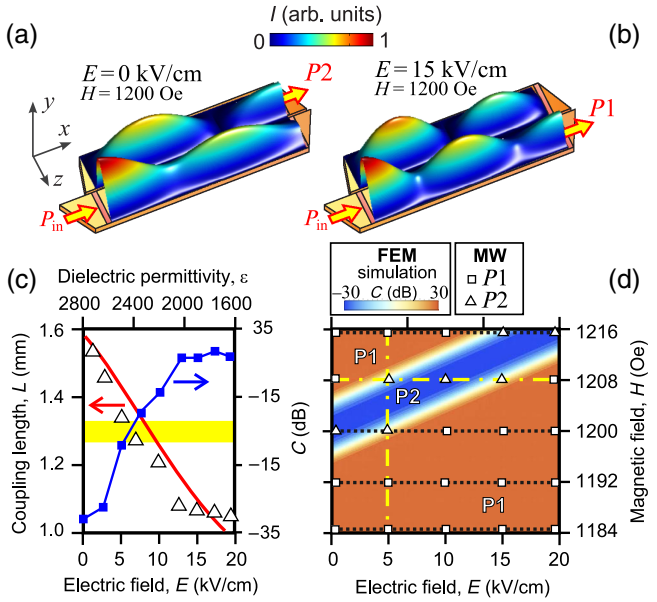

FIG. 4. FEM simulation results. Normalized color-coded intensity map of a HSEW at (a) $E = 0$ kV/cm and (b) $E = 15$ kV/cm. (c) Electric-field dependence of coupling length L and coefficient C. Open triangles show the BLS data. (d) Output regime map $C(E, H)$ of a direction two-channel coupler. Open squares and triangles correspond to the output ports P_1 and P_2. All of the shown data are obtained at the frequency of f_1, and $H = 1200$ Oe.

We note that the dispersion curve for k^{s}_{HE1} intersects the dispersion curve for k^{as}_{HE1} at the frequency $f_i = 5.145$ GHz, denoted by the horizontal dashed line in Fig. 3(a). Therefore, we can conclude that the frequency dependence of the coupling length, which is defined as $L(f) = \pi/|k^{s}_{HE1}(f) - k^{as}_{HE1}(f)|$, has the singularity at f_i; i.e., the small frequency deviation from f_i leads to the intense variation of L. To demonstrate this fact, we perform the BLS measurement of L in the frequency range 5.05–5.3 GHz with a step of 25 MHz [see Fig. 3(b), the open triangles], where $E = 0$ kV/cm. The black triangle corresponds to the frequency $f_1 = 5.15$ GHz. The measured data are consistent with the simulated results [Fig. 3(b), the solid curve]. The coupling length decreases by about a factor of 2 when the frequency is detuned from f_i by about 50 MHz. We emphasize that the coupling length is tuned mainly due to the eigenmode hybridization, not the electric field-dependent ferromagnetic resonance [44]. As seen in Figs. 3(a) and 3(b), the most effective tuning of L is achieved for HSEW with wave numbers in the range of 50–150 cm^{-1}. This correlation explains why the frequency of the second dip, f_2, is not shifted when the dc voltage is applied [Fig. 1(b)]. It should also be noted that the completely monotonic form of $L(f)$ is typical for the side-coupled magnetic stripes [21] [see the dotted curve in Fig. 3(b)], simulated for $\varepsilon = 1$. The numerical simulation confirms the nature of the dip in the transmission of the HSEW. The dashed curves in Fig. 1(b) show the calculated transmission, and Figs. 4(a) and 4(b) demonstrate the calculated distribution of the spin-wave intensity at $E = 0$ kV/cm and $E = 15$ kV/cm.

To confirm the smooth voltage tunability of the coupled multiferroics, we change the electric field to the range 0–20 kV/cm and perform the BLS measurements of the coupling length [shown in Fig. 4(c) by open triangles] at the frequency f_1. Since we know the relation between ε and E, we calculate the coupling length L as a function of E [shown by a solid red curve in Fig. 4(c)]. These data demonstrate that the experimental results are in good agreement with the calculated results, i.e., the monotonic decrease of L with a decrease of ε. We also note that the increase of E from 0 to 12.5 kV/cm leads to an increase of the coefficient C of about 50 dB, which is defined as $C = 10\log(P_1/P_2)$, where $P_1 = \int_0^w I(z)dz$ and $P_2 = \int_{w+d}^{2w+d} I(z)dz$.

IV. DISCUSSION

It is worth noting that the frequency shift $\Delta f = 25$ MHz of the first dip [see Fig. 1(b)] can be achieved not only by varying the electric field from 0 to 15 kV/cm but also by decreasing the value of the bias magnetic field at $\Delta H = \Delta f/\gamma = 8.9$ Oe. From this discussion, we can conclude that the variation of both E and H can affect the spin-wave dynamics in coupled multiferroic stripes. To demonstrate the dual tunability of the tested device, we plot the color-coded regime map $C(E, H)$ in Fig. 4(d) for the frequency f_1. To confirm the validity of the numerically calculated map $C(E, H)$, we perform the MW measurements at the fixed electric and magnetic fields in the range of values shown in Fig. 4(d). We denote by open squares in Fig. 4(d) the regime, which corresponds to the signal output through the port P_1. As the transmission decreases by 5 dB, we mark this point with an open triangle. As has been mentioned above, this intensity drop at the position of port P_1 suggests that the energy is transmitted into the port P_2. Therefore, we conclude that the coupling length—and thus the coupling efficiency—is controlled by the electric and magnetic field. We emphasize that the voltage control of the coupling length in the YIG/BST bilayer is originated mainly by the coupling of the symmetric and antisymmetric modes of the magnetic stripe with the first and second modes in the ferroelectric slab, respectively. Our findings are of particular importance for future applications of coupled multiferroics as dual-channel directional coupler in magnonic networks without the drawbacks inherent in modern semiconductor electronics, such as heatless signal transfer and operation in the terahertz frequency range.

V. CONCLUSION

In this paper, we demonstrate that the efficient coupling of the hybrid spin-electromagnetic waves propagating in the heterostructure bilayer is composed of a ferroelectric

layer and adjacent magnetic stripes. Using the space-resolved BLS technique, we show the voltage-controlled transfer of the spin-wave energy between side-coupled stripes. The effective tuning of the coupling length owes its origin to the hybridization of symmetric and antisymmetric modes of adjacent magnetic stripes with transverse modes of ferroelectric slabs. We demonstrate the electric-field control of the efficiency of the spin-wave power transfer between two magnetic stripes of the layered multiferroic structure due to a change of the dielectric constant of the ferroelectric layer. These features make the studied phenomenon very promising for applications of coupled multiferroics to spin-wave-based integrated circuits as a part of magnonic networks.

ACKNOWLEDGMENTS

Structure fabrication, microwave measurements, and numerical simulation were supported by the Russian Science Foundation (Grant No. 16-19-10283). S. A. N. acknowledges the support of the Russian Science Foundation (Grant No. 14-19-00760). This work was partially supported by the Russian Foundation for Basic Research (Grants No. 16-29-14021, No. 16-29-03120, and No. 16-37-60093,16-37-00217). A. V. S. and S. E. S. acknowledge support from a Scholarship of the President of the Russian Federation (RF) (No. SP-313.2015.5) and a Grant of the President of the RF (No. MK-5837.2016.9).

[1] V. V. Kruglyak, S. O. Demokritov, and D. Grundler, Magnonics, J. Phys. D **43**, 264001 (2010).
[2] V. E. Demidov, S. Urazhdin, A. Zholud, A. V. Sadovnikov, A. N. Slavin, and S. O. Demokritov, Spin-current nano-oscillator based on nonlocal spin injection, Sci. Rep. **5**, 8578 (2015).
[3] S. A. Nikitov, D. V. Kalyabin, I. V. Lisenkov, A. N. Slavin, Y. N. Barabanenkov, S. A. Osokin, A. V. Sadovnikov, E. N. Beginin, M. A. Morozova, Y. P. Sharaevsky, Y. A. Filimonov, Y. V. Khivintsev, S. L. Vysotsky, V. K. Sakharov, and E. S. Pavlov, Magnonics: A new research area in spintronics and spin wave electronics, Phys. Usp. **185**, 1099 (2015).
[4] A. V. Chumak, V. I. Vasyuchka, A. A. Serga, and B. Hillebrands, Magnon spintronics, Nat. Phys. **11**, 453 (2015).
[5] Y. Haiming, O. Kelly, V. Cros, R. Bernard, P. Bertolotti, A. Anane, F. Brandl, F. Heimbach, and D. Grundler, Approaching soft x-ray wavelengths in nanomagnet-based microwave technology, Nat. Commun. **7**, 11255 (2016).
[6] M. I. Bichurin, V. M. Petrov, O. V. Ryabkov, S. V. Averkin, and G. Srinivasan, Theory of magnetoelectric effects at magnetoacoustic resonance in single-crystal ferromagnetic-ferroelectric heterostructures, Phys. Rev. B **72**, 060408 (2005).
[7] J. Das, Y.-Y. Song, N. Mo, P. Krivosik, and C. E. Patton, Electric-field-tunable low loss multiferroic ferrimagnetic-ferroelectric heterostructures, Adv. Mater. **21**, 2045 (2009).
[8] K. Roy, S. Bandyopadhyay, and J. Atulasimha, Hybrid spintronics and straintronics: A magnetic technology for ultra low energy computing and signal processing, Appl. Phys. Lett. **99**, 063108 (2011).
[9] A. Toprak and O. Tigli, Piezoelectric energy harvesting: State-of-the-art and challenges, Appl. Phys. Rev. **1**, 031104 (2014).
[10] R. Verba, V. Tiberkevich, I. Krivorotov, and A. Slavin, Parametric Excitation of Spin Waves by Voltage-Controlled Magnetic Anisotropy, Phys. Rev. Applied **1**, 044006 (2014).
[11] S. Dutta, S.-C. Chang, N. Kani, D. E. Nikonov, S. Manipatruni, I. A. Young, and A. Naeemi, Non-volatile clocked spin wave interconnect for beyond-CMOS nanomagnet pipelines, Sci. Rep. **5**, 9861 (2015).
[12] M. A. Morozova, S. V. Grishin, A. V. Sadovnikov, D. V. Romanenko, Y. P. Sharaevskii, and S. A. Nikitov, Tunable bandgaps in layered structure magnonic crystal-ferroelectric, IEEE Trans. Magn. **51**, 2802504 (2015).
[13] A. V. Sadovnikov, E. N. Beginin, K. V. Bublikov, S. V. Grishin, S. E. Sheshukova, Y. P. Sharaevskii, and S. A. Nikitov, Brillouin light scattering study of transverse mode coupling in confined yttrium iron garnet/barium strontium titanate multiferroic, J. Appl. Phys. **118**, 203906 (2015).
[14] V. B. Anfinogenov, T. N. Verbitskaya, Y. V. Gulyaev, P. E. Zil'berman, S. V. Meriakri, Y. F. Ogrin, and V. V. Tikhonov, Resonant interaction of magnetostatic and slow electromagnetic waves in a composite medium, Sov. Tech. Phys. Lett. **12**, 389 (1986).
[15] V. B. Anfinogenov, T. N. Verbitskaya, P. E. Zil'berman, G. T. Kazakov, S. V. Meriakri, and V. V. Tikhonov, Resonant interaction of magnetostatic backward volume waves with slow electromagnetic waves in ferrite/ferroelectric structures, Sov. Phys. Tech. Phys. **35**, 1068 (1990).
[16] V. E. Demidov, B. A. Kalinikos, and P. Edenhofer, Dipole-exchange theory of hybrid electromagnetic-spin waves in layered film structures, J. Appl. Phys. **91**, 10007 (2002).
[17] F. R. Morgenthaler, Nondispersive magnetostatic forward volume waves under field gradient control, J. Appl. Phys. **53**, 2652 (1982).
[18] C. S. Davies, A. Francis, A. V. Sadovnikov, S. V. Chertopalov, M. T. Bryan, S. V. Grishin, D. A. Allwood, Y. P. Sharaevskii, S. A. Nikitov, and V. V. Kruglyak, Towards graded-index magnonics: Steering spin waves in magnonic networks, Phys. Rev. B **92**, 020408 (2015).
[19] A. Y. Annenkov and S. V. Gerus, Propagation of magnetostatic waves in two coupled channels created by a magnetic field, J. Commun. Technol. Electron. **41**, 196 (1996).
[20] M. A. Morozova, S. V. Grishin, A. V. Sadovnikov, Y. P. Sharaevskii, and S. A. Nikitov, Magnonic bandgap control in coupled magnonic crystals, IEEE Trans. Magn. **50**, 4007204 (2014).
[21] A. V. Sadovnikov, E. N. Beginin, S. E. Sheshukova, D. V. Romanenko, Y. P. Sharaevskii, and S. A. Nikitov, Directional multimode coupler for planar magnonics: Side-coupled magnetic stripes, Appl. Phys. Lett. **107**, 202405 (2015).
[22] A. V. Sadovnikov, E. N. Beginin, M. A. Morozova, Y. P. Sharaevskii, S. V. Grishin, S. E. Sheshukova, and S. A. Nikitov, Nonlinear spin wave coupling in adjacent magnonic crystals, Appl. Phys. Lett. **109**, 042407 (2016).

[23] S. Klingler, P. Pirro, T. Bracher, B. Leven, B. Hillebrands, and A. V. Chumak, Design of a spin-wave majority gate employing mode selection, Appl. Phys. Lett. **105**, 152410 (2014).
[24] A. Khitun, M. Bao, and K. L. Wang, Magnonic logic circuits, J. Phys. D **43**, 264005 (2010).
[25] S. Sheshukova, E. Beginin, A. Sadovnikov, Y. Sharaevsky, and S. Nikitov, Multimode propagation of magnetostatic waves in a width-modulated yttrium-iron-garnet waveguide, IEEE Magn. Lett. **5**, 1 (2014).
[26] S. O. Demokritov, B. Hillebrands, and A. N. Slavin, Brillouin light scattering studies of confined spin waves: Linear and nonlinear confinement, Phys. Rep. **348**, 441 (2001).
[27] V. E. Demidov, B. A. Kalinikos, S. Karmanenko, A. Semenov, and P. Edenhofer, Electrical tuning of dispersion characteristics of surface electromagnetic-spin waves propagating in ferrite-ferroelectric layered structures, IEEE Trans. Microwave Theory Tech. **51**, 2090 (2003).
[28] Y. K. Fetisov and G. Srinivasan, Electrically tunable ferrite-ferroelectric microwave delay lines, Appl. Phys. Lett. **87**, 103502 (2005).
[29] A. A. Semenov, S. F. Karmanenko, B. A. Kalinikos, A. N. Slavin, G. Srinivasan, and J. V. Mantese, Ferrite/ferroelectric layered structures for magnetic and electric field tunable microwave devices, Integr. Ferroelectr. **77**, 199 (2005).
[30] A. A. Semenov, S. F. Karmanenko, V. E. Demidov, B. A. Kalinikos, G. Srinivasan, A. N. Slavin, and J. V. Mantese, Ferrite-ferroelectric layered structures for electrically and magnetically tunable microwave resonators, Appl. Phys. Lett. **88**, 033503 (2006).
[31] A. B. Ustinov, G. Srinivasan, and B. A. Kalinikos, Ferrite-ferroelectric hybrid wave phase shifters, Appl. Phys. Lett. **90**, 031913 (2007).
[32] R. W. Damon and J. Eschbach, Magnetostatic modes of a ferromagnet slab, J. Phys. Chem. Solids **19**, 308 (1961).
[33] S. N. Bajpai, Excitation of magnetostatic surface waves: Effect of finite sample width, J. Appl. Phys. **58**, 910 (1985).
[34] A. G. Gurevich and G. A. Melkov, *Magnetization Oscillations and Waves* (CRC Press, London, 1996).
[35] H. Sasaki and N. Mikoshiba, Directional coupling of magnetostatic surface waves in a layered structure of YIG films, J. Appl. Phys. **52**, 3546 (1981).
[36] C. Kittel, Ferromagnetic resonance, J. Phys. Radium **12**, 291 (1951).
[37] S. O. Demokritov and V. E. Demidov, Advances in magnetics, IEEE Trans. Magn. **44**, 6 (2008).
[38] V. E. Demidov and S. O. Demokritov, Magnonic waveguides studied by microfocus Brillouin light scattering, IEEE Trans. Magn. **51**, 0800215 (2015).
[39] H. Haus, *Waves and Fields in Optoelectronics* (Prentice-Hall, Englewood Cliffs, NJ, 1984).
[40] A. V. Sadovnikov, K. V. Bublikov, E. N. Beginin, and S. A. Nikitov, The electrodynamic characteristics of a finite-width metal/dielectric/ferroelectric/dielectric/metal layer structure, J. Commun. Technol. Electron. **59**, 914 (2014).
[41] A. V. Sadovnikov, K. V. Bublikov, E. N. Beginin, S. E. Sheshukova, and S. A. Nikitov, Nonreciprocal propagation of hybrid electromagnetic waves in a layered ferrite-ferroelectric structure with a finite width, JETP Lett. **102**, 142 (2015).
[42] S. O. Demokritov, *Spin Wave Confinement* (Pan Stanford Publishing Ltd., Singapore, 2009).
[43] T. W. O'Keefe and R. W. Patterson, Magnetostatic surface-wave propagation in finite samples, J. Appl. Phys. **49**, 4886 (1978).
[44] Z. Zhou, M. Trassin, Y. Gao, Y. Gao, D. Qiu, K. Ashraf, T. Nan, X. Yang, S. R. Bowden, D. T. Pierce, M. D. Stiles, J. Unguris, M. Liu, B. M. Howe, G. J. Brown, S. Salahuddin, R. Ramesh, and N. X. Sun, Probing electric field control of magnetism using ferromagnetic resonance, Nat. Commun. **6**, 6082 (2015).